

# A Compact Gamma-Ray Detector on CubeSat for the GRID Mission\*

Jia-Xing Wen,<sup>1,2,3</sup> Xu-Tao Zheng,<sup>1,2</sup> Jian-Dong Yu,<sup>4</sup> Yue-Peng Che,<sup>4</sup> Dong-Xin Yang,<sup>5</sup> Huai-Zhong Gao,<sup>1,2</sup> Yi-Fei Jin,<sup>1,2</sup> Xiang-Yun Long,<sup>5</sup> Yi-Hui Liu,<sup>2</sup> Da-Cheng Xu,<sup>2</sup> Yu-Chong Zhang,<sup>6</sup> Ming Zeng,<sup>1,2,†</sup> Yang Tian,<sup>1,2</sup> Hua Feng,<sup>1,5</sup> Zhi Zeng,<sup>1,2</sup> Ji-Rong Cang,<sup>1,5,2,‡</sup> Qiong Wu,<sup>1,5</sup> Zong-Qing Zhao,<sup>3</sup> Bin-Bin Zhang,<sup>7,8</sup> Peng An,<sup>4</sup> and on behalf of GRID collaboration

<sup>1</sup>Key Laboratory of Particle and Radiation Imaging (Tsinghua University), Ministry of Education, Beijing 100084, China

<sup>2</sup>Department of Engineering Physics, Tsinghua University, Beijing 100084, China

<sup>3</sup>Science and Technology on Plasma Physics Laboratory,

Laser Fusion Research Center, CAEP, Mianyang 621900, Sichuan, China

<sup>4</sup>School of Electronic and Information Engineering, Ningbo University of Technology, Ningbo 315201, China

<sup>5</sup>Department of Astronomy, Tsinghua University, Beijing 100084, China

<sup>6</sup>Department of Physics, Tsinghua University, Beijing 100084, China

<sup>7</sup>Key Laboratory of Modern Astronomy and Astrophysics (Nanjing University),

Ministry of Education, Nanjing 210093, Jiangsu, China

<sup>8</sup>Nanjing University, School of Astronomy and Space Sciences, Nanjing 210093, Jiangsu, China

Gamma-Ray Integrated Detectors (GRID) is a student project designed to use multiple gamma-ray detectors carried by nanosatellites (CubeSat), forming a full-time and all-sky gamma-ray detection network to monitor the transient gamma-ray sky in the multi-messenger astronomy era. A compact CubeSat gamma-ray detector has been designed and implemented for GRID, including its hardware and firmware. The detector employs four  $\text{Gd}_2\text{Al}_2\text{Ga}_3\text{O}_{12} : \text{Ce}$  (GAGG:Ce) scintillators coupled with four silicon photomultiplier (SiPM) arrays to achieve a high detection efficiency of gamma rays between 10 keV and 2 MeV with low power and small dimensions. The first detector designed by the undergraduate student team onboard a commercial CubeSat was launched into a Sun-synchronous orbit on 29 October 2018. The detector has been in a normal observation state and accumulated data for approximately 1 month after on-orbit functional and performance tests in 2019.

Keywords: gamma-ray bursts, scintillation detectors, SiPM, CubeSat

## I. INTRODUCTION

Gamma-Ray Integrated Detectors (GRID) is a student project with the scientific purpose of monitoring the transient gamma-ray sky in the local universe, in particular, to accumulate a sample of gamma-ray bursts (GRBs) associated with gravitational waves (GWs). According to the estimation of the joint detection event rate of GW-GRBs, the maximum number of events that can be detected is more than a dozen per year. Therefore, GRID is designed to serve as a full-time, all-sky gamma-ray detection network without Earth occultation or interruptions due to South Atlantic Anomaly (SAA) passes with many compact and modularised gamma-ray detectors on a fleet of CubeSats in low Earth orbit. As a distributed system, GRID can localize the detected GRBs by means of triangulation or flux modulation with simple scintillation detectors[1].

The scientific payloads of GRID are many modularised compact gamma-ray detectors. Many key technologies have been utilised to optimise gamma-ray detection performance in the limited space of a CubeSat. In the first gamma-ray detector prototype of GRID, GAGG:Ce was used and the package was optimised for high transmittance of low-energy X-rays down to 10 keV. To satisfy the limited power and space of

CubeSat, silicon photomultipliers (SiPMs) have been utilised instead of traditional photomultiplier tubes (PMTs) owing to their attractive capabilities such as super miniature size, low weight, low power consumption, and insensitivity to magnetic fields[2]. The high dark noise of the SiPM array restricts the signal-to-noise ratio (SNR) at room temperature; hence, the current sensitive pre-amplifier has been designed, modelled, and optimised to improve the SNR. Data acquisition electronics (DAQ) has been designed based on an off-the-shelf ARM core microcontroller unit (MCU), which is not too complicated for undergraduate students.

The first detector prototype onboard a 6U (30 cm × 20 cm × 10 cm) CubeSat developed by Spacety Co. Ltd, a commercial satellite company in China, was launched into a Sun-synchronous orbit[1], and has been in a normal observation state that accumulated data for approximately 1 month after on-orbit functional and performance tests in 2019. And the second detector with few hardware modifications and improvements was launched into a Sun-synchronous orbit in 2020 and have accumulated data for more than 300 hours of on-orbit observation. A few GRBs have been observed and all the scientific data will be collected and published by the National Space Science Data Center (NSSDC) in the future. In this paper, we present the detailed design of the detector, electronics, and firmware. In addition, the energy resolution, low-energy X-ray detection performance, and high rate performance of the detector are discussed.

\* M.Zeng acknowledges funding support from the Tsinghua University Initiative Scientific Research Program. H.Feng acknowledges funding support from the National Natural Science Foundation of China (Grant Nos. 11633003, 12025301 & 11821303), and the National Key R&D Program of China (Grant Nos. 2018YFA0404502 and 2016YFA040080X).

† Corresponding author, [Ming Zeng, zengming@mail.tsinghua.edu.cn](mailto:Ming Zeng, zengming@mail.tsinghua.edu.cn)

‡ Corresponding author, [Ji-Rong Cang, cangjr14@tsinghua.org.cn](mailto:Ji-Rong Cang, cangjr14@tsinghua.org.cn)

## II. DETECTOR STRUCTURE

A schematic and photograph of the first detector for GRID is shown in Figure 1. The detector comprises four GAGG:Ce scintillators coupled with four SiPM arrays on one SiPM board. Each SiPM array comprises  $4 \times 4$  J-60035-type SiPMs from SensL. The standard output pins of the SiPMs are connected directly in parallel on the front-end electronics (FEE) board. The following DAQ board provides the capabilities of four-channel signal digitisation, power distribution, communication, and detector control. The detector has dimensions of  $5 \text{ cm} \times 9.4 \text{ cm} \times 9.4 \text{ cm}$ , which occupies half of the CubeSat with standard dimensions (units or ‘U’), with a power consumption of  $5 \text{ V} - 0.6 \text{ A}$ . The detector provides the novel electronic interface, supporting the Serial Peripheral Interface (SPI) and Universal Asynchronous Receiver/Transmitter (UART) protocols and pulses per second (PPS) interface. A summary of features of the first detector are listed in Table 1, which makes the detector a modularised CubeSat payload suitable for different nanosatellite platforms.

Table 1. Main features of the first compact gamma-ray detector for GRID.

Detector size	$0.5\text{U}$ ( $9.4 \times 9.4 \times 5 \text{ cm}^3$ )
Weight	780 g
Power	$\leq 3 \text{ W}$
Detection area	$58 \text{ cm}^2$
FOV	$1\pi$
Energy range	$10 \text{ keV} \sim 2 \text{ MeV}$
Dead time	$50 \mu\text{s}$

## III. SCINTILLATOR AND FEE

### A. Scintillator and package

Owing to the limited GAGG:Ce scintillator size available, the detector comprises four GAGG:Ce scintillators to make full use of the area of a standard nanosatellite unit. A single GAGG:Ce scintillator has a surface of  $3.8 \text{ cm} \times 3.8 \text{ cm}$  and a thickness of  $1 \text{ cm}$ . GAGG:Ce has the advantages of high density ( $6.5 \text{ g/cm}^3$ ), providing a high detection efficiency for gamma rays of up to the megaelectronvolt magnitude. The maximum emission spectrum for GAGG:Ce is around  $530 \text{ nm}$ , suitable for silicon-based photodetectors. Its high light yield ( $\sim 30 - 70 \text{ ph/keV}$ ) and  $\sim 100 \text{ ns}$  decay time provide a reasonable SNR when the SiPM arrays are used. The reflection layer is an enhanced specular reflector (ESR), a  $65 \mu\text{m}$  polymer with high reflectance ( $> 98\%$ ) manufactured by 3M. A series of aluminised polyester films, which are usually used as the outermost cover of satellites, should be used as the light shield layer. Owing to the good mechanical characteristics and non-hygroscopic properties of GAGG:Ce[3], no further layers are required to satisfy moisture proofing and mechanical reinforcement. The simplified scintillator package provides high detection efficiency of low-energy X-rays

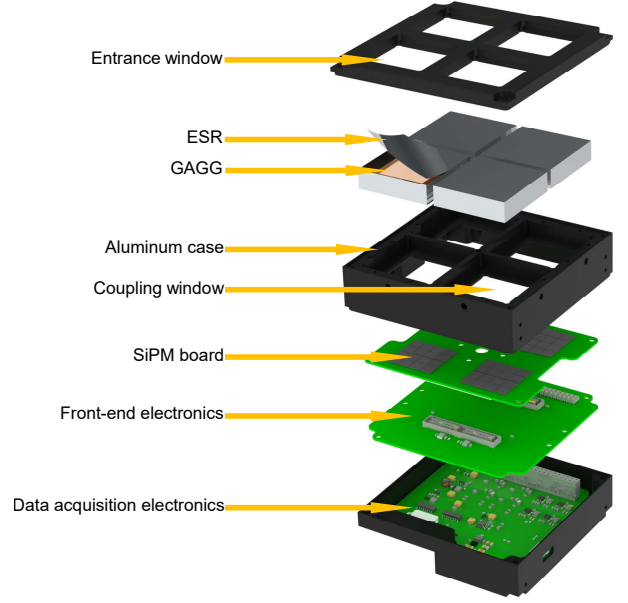


Fig. 1. 3D model of a GRID (top) and photograph of a GRID (bottom)

at a low cost.

With an increase in the number of SiPMs connected in parallel on the same channel, the output capacitance and dark count rate of the SiPM array increase, which reduces the SNR. Therefore, a SiPM array smaller than the bottom area of the scintillator is utilised, similar to many detectors where the scintillator is coupled with SiPM. ESR is cut into a particular shape and covers all of the top and side of the scintillator, and there is a  $2.2 \text{ cm} \times 2.2 \text{ cm}$  square window in the centre of the bottom for the scintillation light collection, as shown in Figure 2. By calibrating the  $661.7 \text{ keV}$  full-energy peak of the  $^{137}\text{Cs}$  source, the light collection efficiency of this kind of package will decrease to  $62\%$ , whereas the efficiency is considered as  $100\%$  using a full coupling of the scintillator bottom surface.

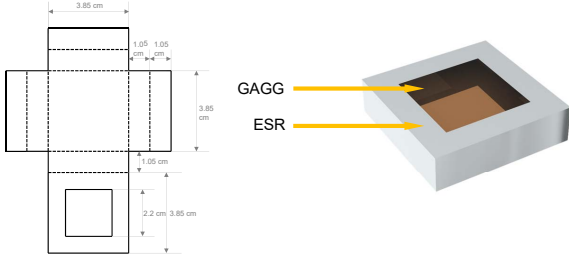


Fig. 2. ESR package (left), where the solid line is the outline and the dashed line is the crease. Bottom view of the GAGG:Ce scintillator with the ESR package (right). ESR is wrapped directly on the scintillator and taped on the side and bottom.

### B. SiPM

The SiPM has many attractive features, such as small size, insensitivity to magnetic fields, low power consumption, and lightweight, which are crucial for applications in space missions[2], especially for nanosatellites. Therefore, four SiPM arrays are utilised as photoelectric converters. The SiPMs are the J-60035 type manufactured by SenSL, which shows a high photon detection efficiency (PDE) curve with reasonable match with the emission spectrum of GAGG:Ce with a low dark count rate. Each SiPM chip has a geometry of  $6.13 \text{ mm} \times 6.13 \text{ mm} \times 0.6 \text{ mm}$ , consisting of 22,292 single-photon avalanche diodes with a microcell fill factor of 75%. The bias voltage supplied to the SiPM is 28.5 V, much lower than what is needed for a PMT. To reduce the dark noise and output capacitance of the SiPM array and control the costs, a  $4 \times 4$  SiPM array is adopted with a  $2.45 \text{ cm} \times 2.45 \text{ cm}$  area, which covers approximately one-third of the area of the bottom of the GAGG:Ce scintillator as mentioned previously.

Four SiPM arrays are integrated on a single board that we designed and manufactured ourselves (Figure 3), and a through silicon via (TSV) package of the SiPM makes the SiPM fill factor of the printed circuit board (PCB) footprint over 93%. Each array is powered independently, and the fast output and standard output of every single SiPM chip is independently extracted to FEE through a high-density connector QTE\_040\_03\_F\_D\_A manufactured by SamTech. Because the breakdown voltage of the SiPM changes with temperature, which affects the gain of the SiPM, there is a temperature-monitoring chip on the other side of the PCB for the correction of the SiPM gain.

### C. FEE

A schematic of the FEE is shown in Figure 4. The standard output signals from one  $4 \times 4$  SiPM array are directly shorted on the FEE and fed to a transimpedance amplifier (TIA) by means of alternating-current (AC) coupling, and the fast output signal pins are left floating. A  $2 \text{ k}\Omega$  resistor connects the standard output of the array to the ground as the direct-

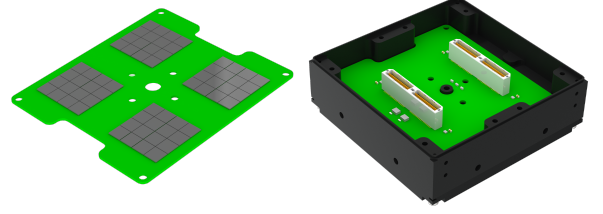


Fig. 3. Top view (left) and bottom view (right) of the SiPM array board

current (DC) path of the standard output, which can restrain the current of the SiPM array to improve the system robustness. A standard high-speed amplifier OPA656 was adopted as the TIA amplifier, and the parameters of the TIA were optimised by detector modelling, as described in the next section. The TIA is followed by a low-pass filter circuit to reverse the signal and adjust the signal amplitude. The filter output is divided into two paths, which are connected with the trigger and peak hold circuit. The trigger circuit is composed of a hysteresis comparator with an adjustable threshold and a monostable pulse generator LTC6993 generating a high-level trigger signal for  $2 \mu\text{s}$  without a retrigger. The high-bandwidth peak hold circuit is composed of an operational transconductance amplifier (OTA) OPA615 and an electronically controlled analogue switch for discharge. Then, the four triggers and four peak hold signals are fed to the DAQ through a standard 2.54 mm connector.

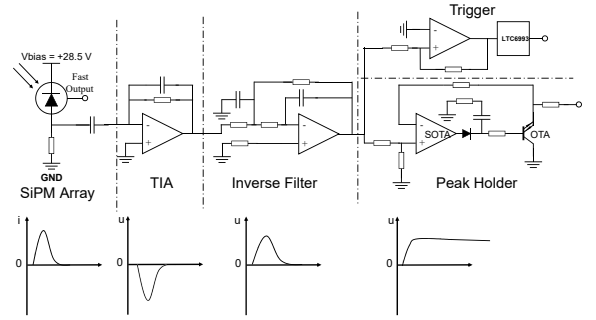


Fig. 4. Functional block diagram and output pulse shape of the FEE for one channel of the GRID

### D. Detector optimization

For such a compact detector, many efforts have been made to improve the SNR, such as the scintillator reflector design, SiPM array design, and high-speed amplifier use. However, we do not have many choices about the scintillator and SiPM, whereas the TIA parameters will significantly affect the SNR and can be analysed and optimised in detail.

The transient response of the GAGG:Ce scintillator can be

expressed as a single exponential decay signal, and the normalised transfer function is

$$H_G(s) = \frac{1}{s \times \tau_{GAGG} + 1} \quad (1)$$

where  $\tau_{GAGG} = 100$  ns is the decay time of GAGG:Ce.

The accurate electrical model of SiPM is a little complicated, but neglecting the equivalent input resistance of the FEE and the quench capacitance can reduce the transient response of the SiPM to a single exponential decay signal, and the normalised transfer function can be expressed as

$$H_S(s) = \frac{1}{s \times \tau_{SiPM} + 1} \quad (2)$$

where  $\tau_{SiPM} \approx 38$  ns is the recovery time of the SenSL J-

series SiPM[4][5].

With proper selection of feedback capacitance and resistance, the TIA can be treated as a second-order Butterworth filter with transfer function

$$H_T(s, R_F) = \frac{\Omega^2 R_F}{s^2 + \frac{\Omega}{Q}s + \Omega^2} \quad (3)$$

where  $\Omega = 2\pi F$ ,  $F = \sqrt{GBP/(2\pi R_F C_D)}$  is the approximate -3 dB bandwidth of the TIA circuit, GBP is the gain bandwidth product of OPA656,  $R_F$  is the feedback resistance, and  $C_D$  is the output capacitance of the SiPM array. Here,  $Q = 0.707$  is the quality factor of the Butterworth filter. Thus, the output pulse waveform of TIA can be expressed as

$$\text{Pulse}(t) = E \times LY \times CE \times PDE \times e \times G \times \mathcal{L}^{-1}[H_G(s)H_S(s)H_T(s)](t) \quad (4)$$

where  $E$  is the incident photon energy,  $LY$  is the light yield of GAGG:Ce,  $CE$  is the scintillation light collection efficiency determined by the scintillator and its packaging,  $PDE$  is the PDE of the SiPM array,  $e$  is the elementary charge, and  $G$  is the gain of the SiPM.

The equivalent output noise voltage of the TIA contributed by the SiPM dark counts can be treated as a random pulse train. The standard deviation of the dark count noise can be

given by Campbell's theorem[6]

$$V_{n_{SiPM}} = \sqrt{\bar{n} \int_{-\infty}^{+\infty} h^2(t)} \quad (5)$$

where  $\bar{n}$  is the dark count rate and  $\bar{n} \approx 90\text{kHz/mm}^2 \times 576\text{mm}^2$  for one SiPM array at  $20^\circ\text{C}$  with an operation voltage of  $28.5$  V and  $h(t)$  is the dark count pulse. The dark count pulse can be considered a Dirac delta pulse  $eG\delta(t)$  convoluted by the SiPM and TIA response function, thus

$$h(t) = eG\mathcal{L}^{-1}[H_S(s)H_T(s)](t) \quad (6)$$

Considering that the output noise of the TIA is bandlimited, the equivalent output noise voltage contributed by the TIA can be estimated by a very simple expression:

$$V_{n_{TIA}} = \sqrt{((I_N R_F)^2 + 4kTR_F + E_N^2 + \frac{(E_N 2\pi C_D R_F F_0)^2}{3}) \times F_0} \quad (7)$$

where  $I_N$  and  $E_N$  are the input current and voltage noise of OPA656, respectively,  $4kTR_F$  is the thermal noise of the feedback resistor, and  $F_0 \approx 1$  MHz is the band-limiting frequency of the TIA and low-pass filter system. Therefore, the SNR can be defined as

$$\text{SNR} = \frac{\max(\text{Pulse}(t))}{\sqrt{V_{n_{SiPM}}^2 + V_{n_{TIA}}^2}} \quad (8)$$

The SNR varies with the feedback resistance  $R_F$ , as shown in Figure 5, and  $R_F$  was set to  $500 \Omega$  to satisfy both the SNR and appropriate gain.

## IV. DATA ACQUISITION AND PROCESSING

### A. Data acquisition electronics

The DAQ board comprises the power regulator, analogue-digital converters (ADCs), MCU, embedded multimedia card (eMMC), and communication interface to process signals from the FEE, supply electricity for all of the analogue and digital devices, supply and control bias voltage of SiPM arrays, process commands, format data for storage, and transmit data to the spacecraft, as shown in Figure 6. The power



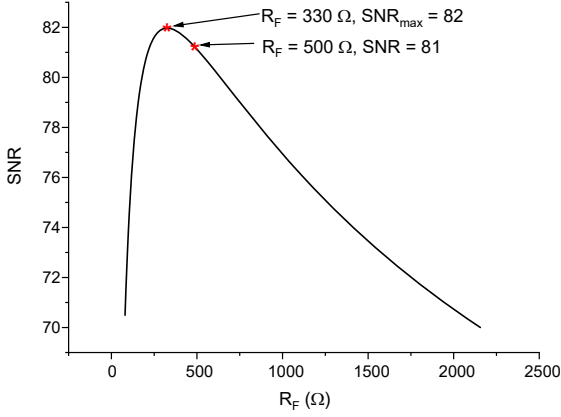


Fig. 5. SNR varying with  $R_F$  when the incident photon energy is 59.5 keV at 20°C with SiPM operating voltage of 28.5 V and scintillator light yield of 32 ph/keV. The maximum value of SNR is 82 at  $R_F = 330 \Omega$ .

system regulates the +5 V input voltage to +5 V and -5 V for the analogue devices, +2.5 V for the ADCs, and +3.3 V for the digital devices. The 0–40 V adjustable bias voltage for the SiPM arrays can be generated through the SiPM bias voltage supply module, which can also monitor the bias voltage and leakage current. The core of the DAQ is a 32-bit ARM Cortex M0+ MCU KEA128 with 16 kB static random access memory (SRAM) and 128 kB flash manufactured by NXP, which is an automotive-level MCU optimised for cost-sensitive applications and focuses on exceptional electromagnetic compatibility (EMC) and electrostatic discharge (ESD) robustness. A 512 MB single-layer cell (SLC) eMMC stores the raw science data and housekeeping data with high reliability. The eMMC can store approximately 12 hours of data based on existing data format definitions and background count rates of 500 counts/s. The peak hold signals from the FEE are sampled by four individual ADCs with 1M sample rates and 16-bit precision, and the four internal ADCs of the MCU are alternatives and can be chosen by a gating switch as redundancy.

As shown in Figure 6, the DAQ electronic provides the interface with the spacecraft, comprising a data bus using differential SPI protocol with LVDS level for the raw science data and housekeeping data transmission, a UART interface for firmware update, a PPS interface for time calibration, and some general-purpose input/output (GPIO) interface for MCU reset, data request, boot configuration, and burst trigger (denoted as Telemetry and RESET).

### B. Flight firmware

The flight firmware operating on the MCU without an operating system comprises two parts, the boot loader and the application program, residing in the internal flash memory of the MCU. The firmware provides limited online data processing capacity because of the low performance of the MCU. However, the configuration of all hardware, response to the

incidents and triggers, command reception and processing, data storage and transmission, control and monitoring of the detector, and the application program update are provided, which can satisfy all necessary in-orbit work requirements.

After the MCU is powered on, the MCU will first run the boot loader to check the Config&Trigger pin's level, and update the application program if high, or jump to the application program if low.

The application program is interrupt driven. Interrupts are generated on the following events:

- (1) FEE trigger;
- (2) timer interruption per second to record housekeeping data;
- (3) PPS from the GPS module;
- (4) spacecraft commands.

When the FEE trigger signals interrupt the MCU, the peak hold signals will be sampled by four individual ADCs or four internal ADCs of the MCU, and the internal clock, PPS count, and UCT time will be recorded. When the converter is finished, the MCU discharges the peak holder. Four channels work in a single thread in the present configuration, so the other channels are in dead time while one channel is triggered. The peak heights and time information are stored in the eMMC. Every 1 s, the MCU records the housekeeping data, as listed in Table 3. The internal clock will be recorded while the PPS triggers the MCU for the accurate time reconstruction of incident photons.

The application program mainly processes the following commands from the spacecraft at present.

- (1) Test communication status.
- (2) Set the bias voltage of each SiPM array and the trigger threshold for each channel.
- (3) Process all modules self-test.
- (4) Update Coordinated Universal Time (UTC).
- (5) Read data from eMMC.
- (6) Read the housekeeping data.
- (7) Set the ADC chosen switch.
- (8) Erase eMMC.

In daily operation, the instruction sequence will be sent to the spacecraft from the Earth station, and then the spacecraft will adjust its attitude, power on the detector, and control the detector to set the SiPM bias voltage starting observation and then power off the detector after a specific observation time. The data stored in the detector eMMC will be read to the POBC's eMMC and downloaded at the appropriate time.

### C. Data format

The DAQ produces two types of data packets: raw science data and housekeeping data. All the raw data will be stored in the eMMC as a series of 512-byte packages. The definitions of raw science data and housekeeping data are shown in Tables 2 and 3, respectively. In a 512-byte raw science data package, the first incident occupies 3–25 bytes, and the

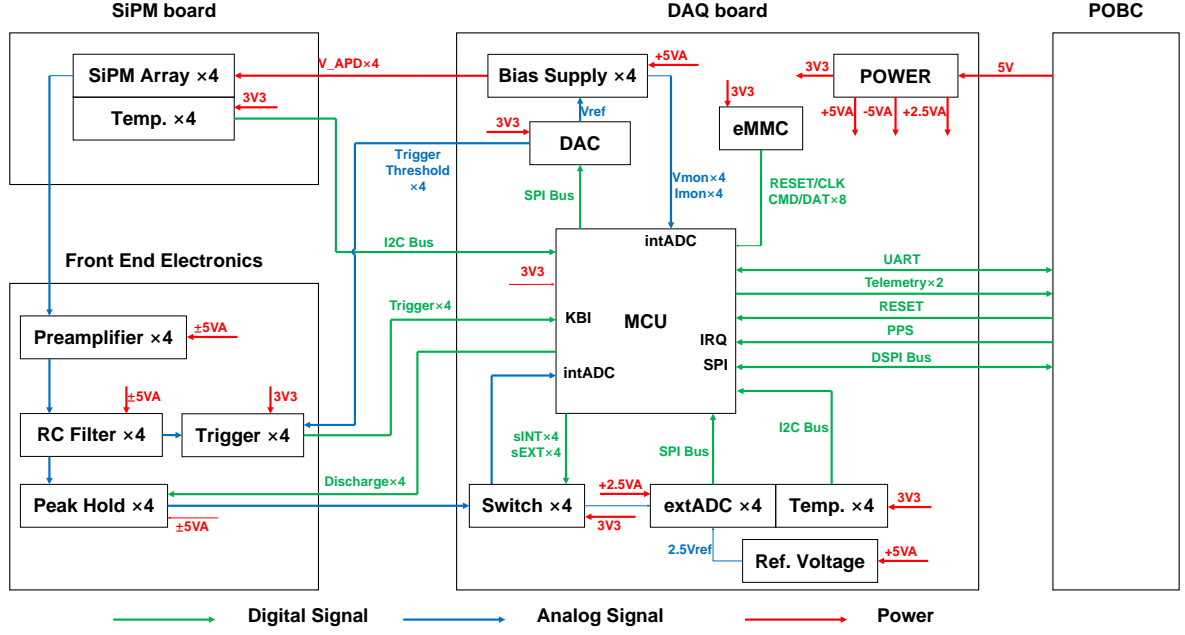


Fig. 6. A functional block diagram of DAQ and its connection with FEE, SiPM Carrier, and payload on-board computer board (POBC). The red lines represent the power bus, the green lines represent the digital signal, and the blue lines represent the analogue signal. The debug interface and TTL-LVDS converter are not shown.

other 43 incidents occupy 26–499 bytes in the same format as shown from 26 to 36 bytes.

Table 2. Raw science data package definition.

Bytes	Content	Bytes	Content
0–2	Head	26	Channel
3	Channel	27–34	Internal clock
4–11	Internal clock	35–36	ADC value
12–13	ADC value	37–499	Incident dataset $\times 42$
14–17	UTC	499–501	Tail
18–25	PPS count	502–503	CRC
		504–511	Vacancy

In a 512-byte housekeeping data package, there are 7 housekeeping datasets occupying bytes 3–492 in the same format as shown in bytes 3–72. ‘UTC’, ‘PPS count’ and ‘Internal clock’ indicate when the housekeeping data package is recorded. ‘PPS to UTC’ indicates the corresponding PPS count last time UTC is received and ‘Internal clock to PPS’ denotes the corresponding internal clock last time PPS is received. From these data, we can precisely correspond the MCU internal clock to the UTC time, which is significant for GRB triangulation.

## V. PERFORMANCE

The performance of detector, including the energy-channel relations at different temperatures and biases, space uniformity, energy resolution, effective areas, angular responses, and detector noise, was calibrated in detail on the ground. The

Table 3. Housekeeping data package definition.

Bytes	Content	Bytes	Content
0–2	Head	55–56	TEMP of MCU
3–6	UTC	57–64	PPS to UTC
7–14	PPS Count	65–72	Internal clock to PPS
15–22	Internal clock	73–492	Telemetry dataset $\times 6$
23–30	TEMP of SiPM $\times 4$	493–495	Tail
31–38	TEMP of DAQ	496–497	CRC
39–46	Bias voltage $\times 4$	498–511	Vacancy
47–54	Leakage current $\times 4$		

detector was irradiated with collimated radioactive sources in the laboratory (from 14 keV to 1.4 MeV) for calibration. Because of the low number of emission lines of radioactive sources below 100 keV, calibration measurements in the energy range from 10 to 60 keV were performed with X-ray radiometry at the National Institute of Metrology of China. The detector calibration results will be described in detail elsewhere in the future. Here, we summarise the key features of low-energy performance, energy resolution, and high rate performance.

### A. Low-energy performance

Through the SNR expression derived previously, assuming that the minimum SNR required is 6, which means that the peak value of the signal amplitude is 6 times the standard deviation of noise, the lower limit for low-energy detection can be derived theoretically. The commercially available

GAGG:Ce has a low light yield of approximately 16 ph/keV for X-ray energy down to 10 keV. Considering normal observation conditions, where the temperature is 20°C, the SiPM operating voltage is 28.5 V, and with a scintillation light collection efficiency of 62%, the PDE of the SiPM array defined by the PDE of a single SiPM multiplied by the array's fill factor of approximately 27.9%, the lower limit of the detector is 13 keV.

The trigger threshold was set to 20 mV (around 13 keV) and a spectrum of  $^{241}\text{Am}$  with 59.5 and 13.5 keV X-rays was measured as shown in Figure 7. The performances of the four channels are not exactly the same owing to the difference in the scintillators' light yield and light collection efficiency, but the peak of the 59.5 keV X-ray can be seen clearly, and the peak at 13.5 keV and the dark count noise are mixed together near the threshold.

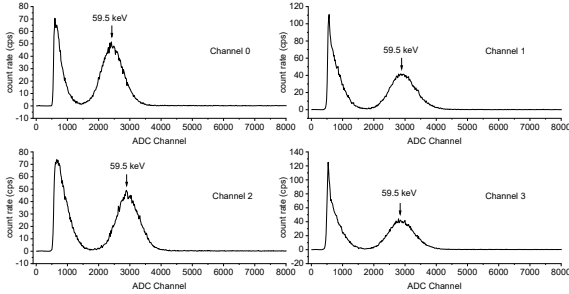


Fig. 7. Spectrum of  $^{241}\text{Am}$  with a trigger threshold of 20 mV of four channels.

### B. Energy resolution

The energy resolution results were calibrated by the radioactive sources in the laboratory that handles the detector and electronics noise as well as the statistical fluctuation and energy nonlinearity. The sources we used for calibration with the energies of their emitted photons are listed in Table 4. As shown in Figure 8, the energy resolution  $\frac{\Delta E}{E}$  is approximately proportional to  $\frac{1}{\sqrt{E}}$  and is approximately 9% at 662 keV. The poor fitting in the low-energy region is due to the nonlinearity of GAGG:Ce, especially the distinct inconsistency at 81 keV, is caused by the X-ray absorption edge of GAGG:Ce at around 70 keV[3].

Table 4. Radioactive sources used for calibration.

Source	Energy (keV)
$^{133}\text{Ba}$	32.1, 81.0
$^{155}\text{Eu}$	41.3
$^{241}\text{Am}$	59.5
$^{22}\text{Na}$	511
$^{137}\text{Cs}$	661.7

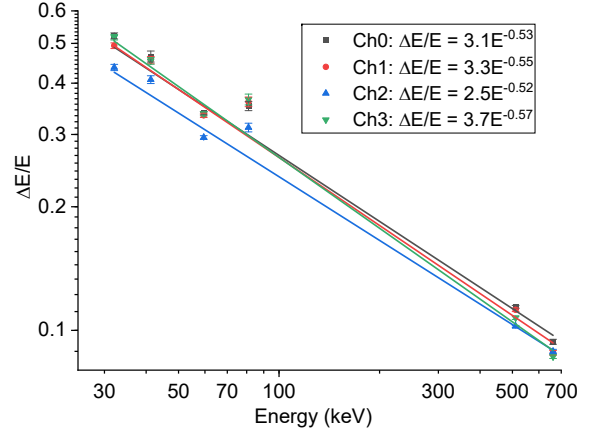


Fig. 8. Dependence of the detector energy resolution of four channels, and the fitting curve and equation with  $y = ax^b$  are shown.

### C. High rate performance

Two effects typically impair the performance of scintillation detectors at high photon rates: dead time and pulse pile-up. Pulse pile-up occurs when the count rate is so high that the pulses from successive events overlap in the FEE, which causes distortions in the measured spectrum that are difficult to characterise, so this kind of distortion is usually treated as systematic errors in the determination of the gamma-ray spectrum. Owing to the high bandwidth of the TIA and filter, the pulse of a single event lasts less than 1  $\mu\text{s}$  from generating a trigger to recovery to baseline, and this will incur little distortion in the measured GRB spectrum according to the relevant discussion about the Fermi GBM detector[7]. However, there is another kind of pulse pile-up occurring at the peak-hold circuit; that is, a small signal will be overridden by a larger signal. This problem can be solved by a limit switch that restricts the peak-hold circuit input voltage to the ground level when this channel is triggered.

The nominal detector dead time is approximately 50  $\mu\text{s}$  per event, which is mainly contributed by the MCU-ADC communication and MCU-eMMC communication, as shown in Figure 9. However, in the last version of firmware, which is used in the second detector of GRID, the dead time has been optimised to 15  $\mu\text{s}$  with the same hardware design.

## VI. CONCLUSION

GRID is a student project with a dedicated and straightforward scientific goal: to detect and locate GRBs produced by neutron star mergers jointly with ground-based GW detectors in the local universe. In this paper, the detailed design of the GRID detector, electronics, and firmware as well as the energy resolution and low-energy and high-rate performance of the detector have been introduced. Further calibration of the detector, including the angular response, detection efficiency, and temperature response with both simulation and experi-

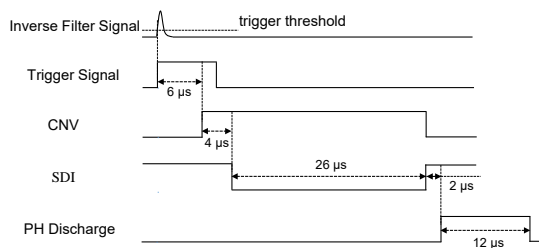


Fig. 9. Contribution of dead time in a GRID. When the MCU is triggered by the FEE trigger output signal, a conversion input (CNV) will be generated after 6  $\mu$ s to initiate the ADC conversions. The ADC conversion takes 4  $\mu$ s, following which there is a 26  $\mu$ s MCU-ADC SPI communication time. Then, the discharge signal is generated after 2  $\mu$ s and lasts for 12  $\mu$ s until the ADC value is wrapped in eMMC.

ments, will be reported elsewhere in detail.

As mentioned previously, GRID was initially proposed and developed by students, with a considerable contribution from undergraduate students, and will remain operating as a student project in the future. The current GRID collaboration involves more than 20 institutions and continues to grow. The purpose of GRID is twofold. In addition to its scientific goals, we hope to attract excellent students from different disciplines into astrophysics and train them on organising and participating in a multi-discipline collaboration, while learning how to build a real science project that covers hardware, data, and science. In conclusion, GRID is a scientific collaboration that accepts students and scientists from all over the world; the members can launch their own detectors, share the data, and produce scientific results under certain agreements. The detailed hardware and firmware design materials described in this paper will be part of a standard design package to be delivered and shared inside the GRID collaboration.

- 
- [1] J. Wen, X. Long, X. Zheng, et al., GRID: a student project to monitor the transient gamma-ray sky in the multi-messenger astronomy era, *EXPERIMENTAL ASTRONOMY* 48 (1) (2019), pp. 77–95.
  - [2] V. Bindi, A. D. Guerra, G. Levi, L. Quadrani, C. Sbarra, Preliminary study of silicon photomultipliers for space missions, *Nuclear Inst & Methods in Physics Research A*, 572 (2) (2007), pp. 662–667.
  - [3] J. Iwanowska, L. Swiderski, T. Szczesniak, P. Sibczynski, M. Moszynski, M. Grodzicka, K. Kamada, K. Tsutsumi, Y. Usuki, T. Yanagida, Performance of cerium-doped  $\text{Gd}_2\text{O}_3$  scintillator in gamma-ray spectrometry, *Nuclear Inst & Methods in Physics Research A*, 712 (6) (2013), pp. 34–40.
  - [4] D. Marano, G. Bonanno, M. Belluso, S. Billotta, A. Grillo, S. Garozzo, G. Romeo, A. D. Grasso, S. Pennisi, G. Palumbo, A New Accurate Analytical Expression for the SiPM Transient Response to Single Photons. 21st IEEE International Conference on Electronics, Circuits and System (Ieee, New York, 2014), pp. 514–517.
  - [5] A. N. Otte, D. Garcia, T. Nguyen, D. Purushotham, Characterization of three high efficiency and blue sensitive silicon photomultipliers, *Nuclear Inst & Methods in Physics Research A*, 846 (2017), pp. 106–125.
  - [6] L. Cohen, Generalization of Campbell's theorem to nonstationary noise. 22nd European Signal Processing Conference (EU-SIPCO) (2014), pp. 2415–2419.
  - [7] Meegan, Charles, et al. The Fermi Gamma-Ray Burst Monitor. *The Astrophysical Journal*, 702.1(2009):791.